Unconserved substrate-binding sites direct stereoselectivity of medium-chain alcohol dehydrogenase

Shanshan Wang,‡[a] Yao Nie,‡[a] Yan Xu,*[a] Rongzhen Zhang,[a] Tzu-Ping Ko,[b] Chun-Hsiang Huang,[c] Hsiu-Chien Chan,[c] Rey-Ting Guo*[c] and Rong Xiao[d]

[a] *School of Biotechnology and Key laboratory of Industrial Biotechnology, Ministry of Education, Jiangnan University, Wuxi 214122, China. E-mail: yxu@jiangnan.edu.cn; Fax: +86-510-85864112; Tel: +86-510-85918201*
[b] *Institute of Biological Chemistry, Academia Sinica, Taipei 11529, Taiwan*
[c] *Industrial Enzymes National Engineering Laboratory, Tianjin Institute of Industrial Biotechnology, Chinese Academy of Sciences, Tianjin 300308, China. E-mail: guo_rt@tib.cas.cn; Fax: +86-022-84861926; Tel: +86-022-84861999*
[d] *Center for Advanced Biotechnology and Medicine, Rutgers University, Piscataway, NJ 08854, USA*

‡ *These authors contributed equally to this work.*

Supplementary Information

Table of Contents

1. Chemical Materials

Ketones (**1a-8a**), alcohols ((*S*)-**1b**, (*R*)-**1b**, (*S*)-**4b**, (*R*)-**4b**), NADH and NAD^+ were purchased from Sigma-Aldrich Chemical Co., USA. All other racemic alcohol standards were prepared by reduction of ketones with sodium borohydride. The enzymes, vectors, oligonucleotides and other reagents for DNA cloning and amplification were from Takara-Bio Co., Japan and Novagen Co., USA. Hexane and isopropanol used for High Performance Liquid Chromatography (HPLC) were of chromatographic grade (Honeywell Co., USA). All other chemicals used were of analytical grade and commercially available.

2. Construction, expression and purification of RCR WT and variants

The gene encoding RCR from *C. parapsilosis* was cloned into the pET32 Xa/LIC vector, and the recombinant plasmid was called pET32-RCR. The plasmid was amplified using the protocol from the Agilent QuikChange Lightning Site-Directed Mutagenesis Kit. The primers were shown in Table S3. Plasmid DNA was prepared and sequenced to confirm the positive clones. The recombinant plasmid was transformed to *Escherichia coli* BL21 *trxB* (DE3). Cells were grown in LB medium containing 100 μg mL^{-1} ampicillin, 50 μg mL^{-1} kanamycin and 0.2 mM zinc acetate. The protein was expressed without induction of isopropyl β-D-1-thiogalactopyranoside (IPTG) at 28 °C for 12 hours.[1] Cells were harvested by centrifugation at 7,000 x *g* and resuspended in a lysis buffer containing 25 mM Tris-HCl, 150 mM NaCl and 20 mM imidazole, pH 8.0. Cell lysate was prepared with a French Press Instrument, and then centrifuged at 17,000 x *g* to remove cell debris. The proteins were purified by FPLC using a Ni-NTA column. The buffer and gradient for the Ni-NTA column were 25 mM Tris-HCl, 150 mM NaCl, and 20-500 mM imidazole, pH 8.0. His-tagged RCR was eluted at about 120 mM imidazole. The protein solution was dialyzed against a buffer containing 25 mM Tris-HCl, 150 mM NaCl, pH 8.0, and then subjected to Factor Xa digestion to remove the His tag. The mixture was then passed through Ni-NTA column again and the untagged RCR was eluted with 5 mM imidazole-containing buffer. The purified protein was finally concentrated to 10 mg mL^{-1} in a 25 mM Tris-HCl, 150 mM NaCl, pH 8.0 buffer. The preparation procedure of H49A, F285A, W286A, and F285A/W286A variants was almost identical to that of WT protein.

3. Crystallization, data collection, structure determination and refinement

The RCR WT protein was first crystallized by using the Hampton Research Crystal Screen kits and sitting-drop vapor diffusion method. However, we failed to yield the crystals of *apo*-RCR in the absence of its cofactor (NAD^+). Then RCR was co-crystallized with NAD^+. The reservoir solution (PEG/Ion 2 screen kit, No. 7) contained 0.10 M sodium malonate pH 7.0, and 12%(*w/v*) PEG 3350. Better crystals were obtained by optimizing the reservoir composition, which contained 0.10 M sodium malonate pH 7.0, 12%(*w/v*) PEG 3350 and 2%(*w/v*) PEG 10000. All crystals were prepared at room temperature. They reached suitable sizes for X-ray diffraction in 1-2 days. Then the crystals were soaked in cryoprotectant solution (0.15 M sodium malonate pH 7.0, 20%(*w/v*) PEG 3350, 5%(*w/v*) PEG 10000 and 10%(*w/v*) glycerol), and then used for data collection to obtain the binary complex with NAD^+. Considering the ternary complex with cofactor and substrate/product, the *holo*-crystal had been soaked in cryoprotectant solution containing additional saturated (*R*)-**1b** for 30 min. In addition, the RCR_H49A mutant, destroyed the proton-relay system, was also co-crystallized with NAD^+ and the reservoir solution contained 0.10 M BIS-TRIS pH 6.5, 18%(*w/v*) PEG 1500 and 8%(*w/v*) PEG 3350. Then the crystals were soaked by the cryoprotectant solution comprised of 0.10 M BIS-TRIS pH 6.5, 20%(*w/v*) PEG 1500, 10%(*w/v*) PEG 3350, 5%(*w/v*) glycerol and saturated **1a**. Unexpectedly, the electron density maps revealed that (*R*)-**1b** indeed entered into the substrate-binding pocket while the bound NAD^+ was released. This result might be interpreted as the following process: 1) (*R*)-**1b** was bound to the substrate-binding pocket of RCR; 2) RCR catalyzed (*R*)-**1b** to produce **1a**, and subsequently **1a** and NAD(H) were dissociated; 3) (*R*)-**1b** at high concentration re-entered the pocket. Consequently, we obtained the binary complex with (*R*)-**1b** at 2.30 Å resolution. Similarly, soaking **1a** of the H49A mutant crystals also obtained the binary complex with **1a** at 2.95 Å resolution, owing to maintenance of a small amount of activity.

The X-ray diffraction data sets were collected at beam lines BL13B1 and BL13C1 of the National Synchrotron Radiation Research Center (NSRRC, Hsinchu, Taiwan). The diffraction images were processed using the program HKL-2000.[2] Prior to use in structural refinements, 5% randomly selected reflections were set aside for calculating R_{free} as a monitor. Structure of RCR-NAD^+ were solved by molecular replacement (MR) using a high homologous ADH from *Rhodococcus rubber* (31.5% identity, PDB code 2XAA), and the other two structures were solved by MR using structure-known *holo*-RCR. All of the following structural refinements were carried out using the programs CNS[3] and Coot[4]. Data collection and refinement statistics of these crystals were summarized in Table S2. All diagrams of protein structures were prepared by using the software PyMOL (http://www.pymol.org/). The three RCR coordinates have been deposited in the Protein Data Bank: 3WLE (RCR-NAD^+ complex), 3WLF (RCR-(*R*)-**1b** complex), 3WNQ (RCR_H49A-**1a** complex).

4. Description of the overall protein structure

The overall structure of RCR-NAD^+ complex revealed as a homo-tetramer, a dimer of dimers. Like other NADH-dependent MDRs, each RCR subunit was composed of a cofactor-binding domain (residues 155-284) and a catalytic domain (residues 1-154, 285-336). The cofactor-binding domain contained a Rossmann-fold motif, which was comprised of a six stranded parallel β-sheet (βA-βF), surrounded by five α-helices (αA-αE). The core of the catalytic domain was a ten-stranded β-sheet of mixed type (β1-β10), with six helical segments situated on the surface (α1-α6) (Fig. S1). The structural zinc ion was coordinated by four Cys (95, 98, 101 and 109) to stabilize the conformation of RCR. The catalytic zinc ion was positioned at the bottom of the hydrophobic substrate-binding pocket, coordinated by three residues (Cys44, His65 and Asp154) and a water molecule. The fourth coordination was alterable in the different states of reaction. The zinc bound water molecular in RCR-NAD^+ complex was replaced by the Oe1 atom of Glu66 in RCR-(*R*)-**1b** complex. Although we failed to obtain the ternary complex, the hydroxyl oxygen atom of (*R)*-**1b** might be the fourth ligand in accordance with the pervious report of MDRs.[5]

NAD$^+$ was located inside a cleft formed between two domains. Amino acid residues (H5, S46, H49, G181, L182, V260, L262, S284, W286, N326 and R331) made hydrogen bonds to stabilize the cofactor binding, and the other residues (C44, D154, T158, G180, D201, K202, L203, A206, F237, V238, T243, G261, F285 and L323) formed the hydrophobic interactions with NAD$^+$ (Fig. S2). These functional residues interacting with NAD(H) are similar to those found in other structure-solved MDRs in accordance with the multi-sequence alignment (Fig. S6). Four sequence motifs for NAD(H) binding in MDR family are identified as C-[HRG]-[ST]-x(2)-H, [DC]-x(3)-T-x(20, 25)-G-G-[LV]-x(18, 19)-D, [TA]-x(16, 17)-V-G-[LV] and [LM]-x(6, 8)-R, which provides insight into the interaction of NAD(H) with structure-unknown MDRs. In addition, cofactor binding induced the conformational change from an open state to a closed state, involving a rotation of the catalytic domain relative to the cofactor-binding domain to produce a catalytically efficient enzyme (Fig. S3).[6]

5. Determination of kinetic parameters

The enzyme assay mixture in 100 μL for the reductive activity of the purified RCR WT and variants comprised 0.1 M potassium phosphate buffer (pH 6.5), 5 mM $ZnCl_2$, 1 mM NADH, 5 mM substrates, and an appropriate amount of the enzymes. The decrease in NADH absorbance at 340 nm was recorded for 3 min at 30 °C. The molar extinction coefficient of NADH was 6,220 L mol^{-1} cm^{-1}. One unit (U) of enzyme activity was defined as 1 μmol of NADH consumed per minute under the assay conditions. Kinetic parameters of WT and variants were assayed by measuring initial velocity at various concentrations of substrates and cofactors. Various concentrations of substrates (**1a-8a**) (0.1-8 mM), enzyme (10 μM) and NADH (0.05-0.25 mM) in 0.1 M potassium phosphate buffer (pH 6.5) were used. The kinetic parameters were further calculated from double reciprocal Lineweaver–Burk plots based on Theorell-Chance Bi-Bi reaction kinetics. All measurements were made in triplicate. The protein concentrations were determined by measuring UV absorption at 280 nm, using the molar extinction coefficients of 30,370 M^{-1} cm^{-1} (WT, F285A) and 24,870 M^{-1} cm^{-1} (W286A, F285A/W286A), calculated by ExPASy from the amino acid compositions. The calculated K_m of NADH revealed that the mutations had only subtle change for cofactor affinity (data not shown), so we here focused on the affinity and catalytic property of substrate ketones.

6. General bioconversion and analytical method

The bioconversion mixture in 5 mL comprised 0.1 M potassium phosphate buffer (pH 6.5), 0.5 mM $ZnCl_2$, 0.5 mM NADH, 10 mM substrates, 1‰(*v/v*) isopropanol, and an appropriate amount of the enzymes was shaken at 200 rpm and 30 °C for 3 h. Then, the mixture was extracted with ethyl acetate by vigorous mixing, and the organic layer was filtered through a 0.22 μm PVDF syringe filter (Troody Technology, China) for analysis. The optical purity of products were determined by HPLC (HP

1100, Agilent, USA) equipped with a Chiralcel OB-H column (4.6 mm×250 mm; Daicel Chemical Ind., Ltd., Japan) as described by previous reports.[7] The details of chiral HPLC analysis were showed in Fig. S8-15.

7. Docking experiments

The structure models of variants (F285A, W286A and F285A/W286A) were performed by DeepView 4.1 (http://spdbv.vital-it.ch/). The docking experiments of WT and variants towards **1a**, **3a**, **4a** and (*R*)-**1b** were performed with AutoDock Vina 1.0.[8] A docking algorithm that took account of substrate flexibility but kept the *holo*-protein rigid was employed. Docking runs were carried out using the standard parameters of the program for interactive growing and subsequent scoring, except for the parameters for setting grid box dimensions and center. The values for setting grid box dimensions and centers in docking studies were based on the known substrate-binding pocket.

8. Supplementary Tables and Figures

9. Tables

Table S1. MDR members with stereoselectivity deposited in PDB Bank.

Enzyme	PDB ID	Ligands	Stereoselectivity	Ref.
Human ADH $\alpha\alpha$	1U3T	NAD^+ and CCB	Anti-Prelog	9
Human ADH $\beta_1\beta_1$	1U3U	NAD^+ and BNF	Prelog	9
Human ADH $\gamma_2\gamma_2$	1U3W	NAD^+ and FXY	Prelog	9
Horse liver ADH (HLADH)	4DWV	NAD^+ and PFB	Prelog	10
Mouse ADH2	1E3I	NADH and CXF	Prelog	11
Saccharomyces cerevisiae ADH1 (SceADH1)	2HCY	8ID and ETF	Prelog	12
Sulfolobus solfataricus ADH (SsADH)	1R37	NAD^+ and ETX	Prelog	13
Rhodococcus ruber ADH (ADH-'A')	2XAA	NAD^+ and BU1	Prelog	14
Pseudomonas aeruginosa ADH (PaADH)	1LLU	NAD^+ and EDO	Prelog	15
Clostridium beijerinckii ADH (CbADH)	1KEV	NADPH	Prelog	16
Ralstonia eutropha ADH (FurX)	3S2F	NAD^+ and FU2	Prelog	17
Thermoanaerobacter brockii ADH (TbADH)	1YKF	$NADP^+$	Prelog/Anti-Prelog	18

Table S2. Data collection and refinement statistics of RCR crystals.

	RCR-NAD$^+$	RCR-(*R*)-**1b**	RCR_H49A-**1a**
Data collection			
Space group	$P2_12_12_1$	$P2_12_12_1$	$P2_12_12_1$
Unit cell *a*, *b*, *c* (Å)	85.64, 106.11, 145.55	93.49, 103.72, 141.94	70.33, 93.03, 242.35
Resolution (Å) [a]	25.0-2.15 (2.23-2.15)	25.0-2.30 (2.38-2.30)	30.0-2.95 (3.06-2.95)
Unique reflections	70570 (6948)	62316 (6126)	34016 (3355)
Average Redundancy	4.8 (5.0)	7.2 (6.8)	4.1 (4.1)
Completeness (%)	99.9 (99.8)	99.9 (99.5)	99.2 (99.2)
Average $\langle I \rangle / \langle \sigma(I) \rangle$	20.7 (5.3)	30.1 (6.6)	20.2 (3.0)
R_{merge} (%)	9.2 (37.7)	9.2 (37.8)	8.7 (49.8)
Refinement			
No. of reflections	68025 (4606)	60076 (5701)	31629 (2523)
R_{work} (95% data)	0.181 (0.242)	0.205 (0.244)	0.230 (0.375)
R_{free} (5% data)	0.216 (0.282)	0.249 (0.314)	0.288 (0.387)
RMSD bonds (Å)	0.006	0.004	0.007
RMSD angles (°)	1.40	1.03	1.51
Ramachandran (%) [b]			
Favored	96.1	93.6	90.6
Allowed	3.9	5.8	8.8
Outliers	0	0.5	0.6
$B_{average}$ (Å^2)/atoms			
Protein	29.2/10085	29.8/10040	82.6/10068
Ligands	23.8/184	37.7/48	91.4/48
Water	37.9/1076	39.3/1073	55.1/229
PDB code	3WLE	3WLF	3WNQ

[a] Numbers in parentheses are for the outermost resolution shells. [b] Calculated by using MolProbity.[19]

Table S3. PCR primers for cloning and site-directed mutagenesis with mutated bases underlined.

Construct	Primer	Sequence (5'-3')
WT	WT_F	GGTATTGAGGGTCGCGCGGGCGCGGGCGCGATGTCAATTCCATCAAGCCAGTACGGATT
	WT_R	AGAGGAGAGTTAGAGCCCTATGGATTAAAAACAACTCTACCTTCATAAG
H49A	H49A_F	TTGTGTCATTCTGATTTA**GCG**GTCATTTACGAAGGGTTG
F285A	F285A_F	CGAATCTTGGGTAGT**GCG**TGGGGAACTACTAATGATTTGG
W286A	W286A_F	CGAATCTTGGGTAGTTTT**GC**GGGAACTACTAATGATTTGG
F285A/W286A	F285A/W286A_F	CGAATCTTGGGTAGT**GCGGC**GGGAACTACTAATGATTTGG

Table S4. Kinetic parameters for RCR WT and vairants with aryl ketones.

No.	WT			F285A			W286A			F285A/W286A		
	K_m (mM)	k_{cat} (s^{-1})	k_{cat}/K_m (mM^{-1} s^{-1})	K_m (mM)	k_{cat} (s^{-1})	k_{cat}/K_m (mM^{-1} s^{-1})	K_m (mM)	k_{cat} (s^{-1})	k_{cat}/K_m (mM^{-1} s^{-1})	K_m (mM)	k_{cat} (s^{-1})	k_{cat}/K_m (mM^{-1} s^{-1})
1a	0.95	7.00	7.37	1.53	5.40	3.53	0.88	6.46	7.34	0.86	5.33	6.20
2a	0.80	3.01	3.76	0.22	2.50	11.36	0.18	1.46	8.11	0.15	1.88	12.53
3a	0.97	1.39	1.43	0.89	0.96	1.08	0.45	1.57	3.49	0.43	1.42	3.30
4a	0.56	7.42	13.25	0.65	6.51	10.02	0.63	7.30	11.59	0.67	6.83	10.19
5a	1.10	2.28	2.07	1.87	3.84	2.05	0.71	1.83	2.58	0.71	3.96	5.58
6a	1.29	1.53	1.19	2.23	8.44	3.78	0.95	2.04	2.15	0.85	3.30	3.88
7a	1.67	2.09	1.25	0.69	3.30	4.78	1.53	8.85	5.78	0.93	9.15	9.84
8a	0.58	0.83	1.43	0.21	1.53	7.29	0.17	1.27	7.47	0.19	1.63	8.58

10. Figures

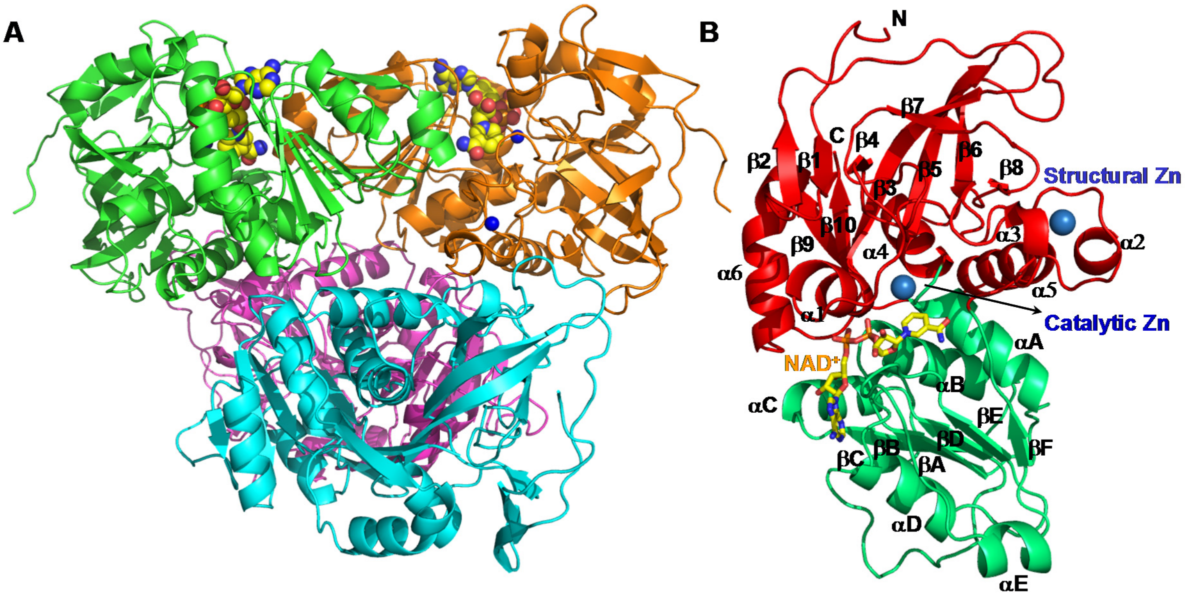

Figure S1. Overall of the binary structure of RCR with NAD$^+$. A: Arrangement of the tetrameric RCR. Each dimer, green:orange or magenta:cyan, was composed of two subunits connected by the continuous 12-stranded β-sheet. Only one dimer showed NAD$^+$ in sphere (yellow). B: The catalytic domain (red) and cofactor-binding domain (green) of RCR monomer. The catalytic and structural Zn ions were depicted with spheres (blue). Bound NAD$^+$ in the cleft of two domains was shown in stick (yellow).

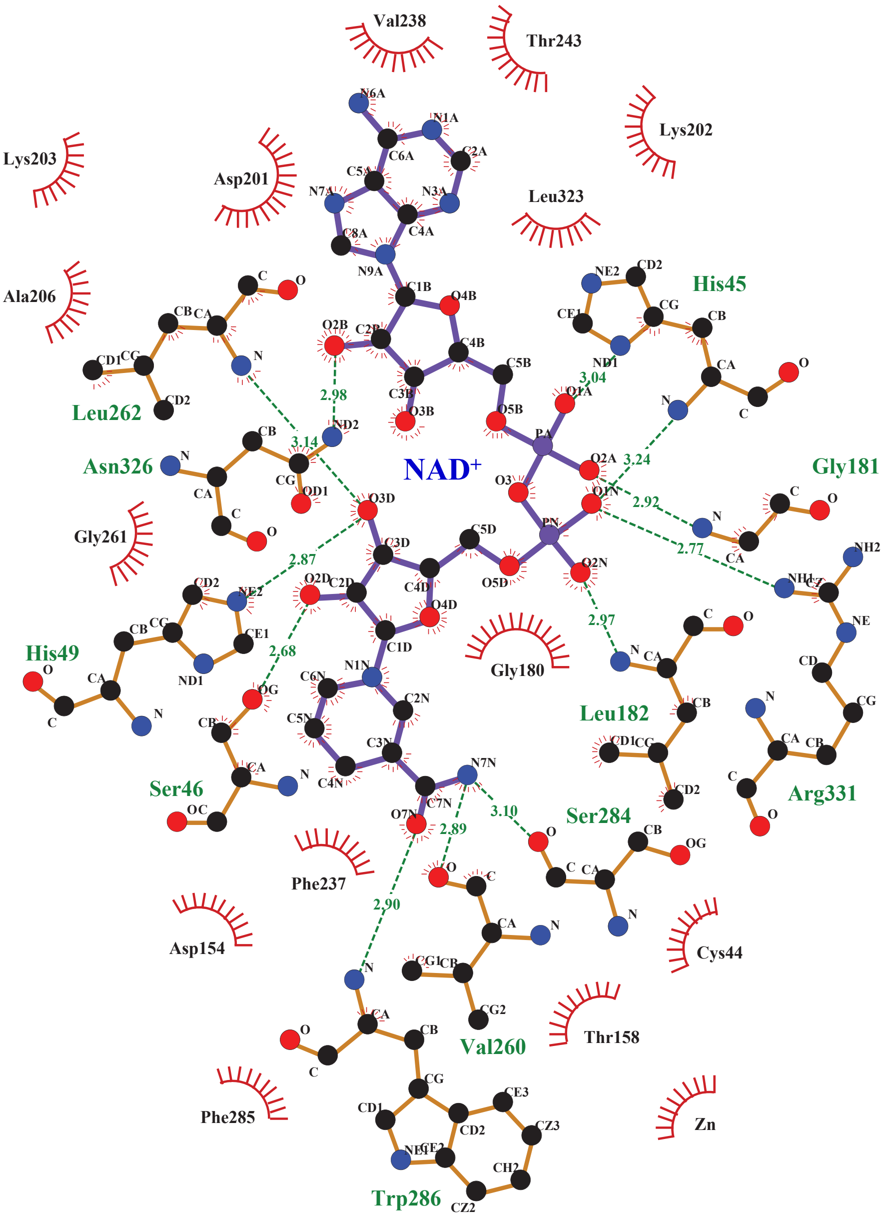

Figure S2. Interactions between NAD^+ and the amino acid residues of RCR.

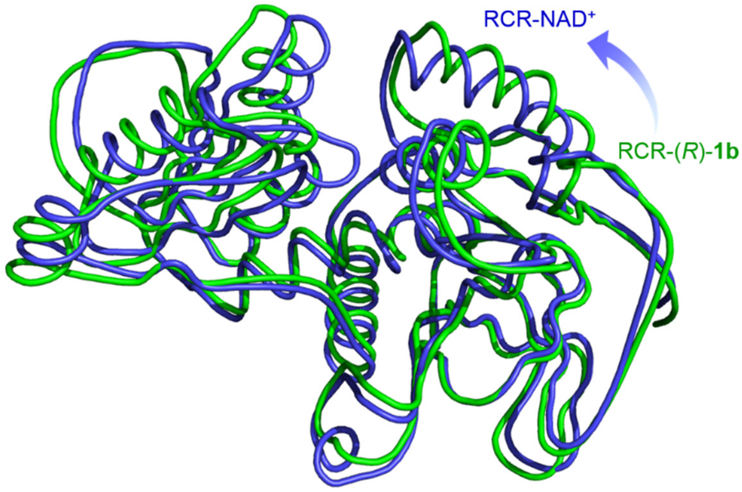

Figure S3. Structural comparison of monomer RCR-NAD$^+$ (blue) with RCR-(*R*)-**1b** (green) used by iPBA (http://www.dsimb.inserm.fr/dsimb_tools/ipba/).[20] The Cα atoms had average root mean square deviations (rmsd) of 1.82 Å between the two structures.

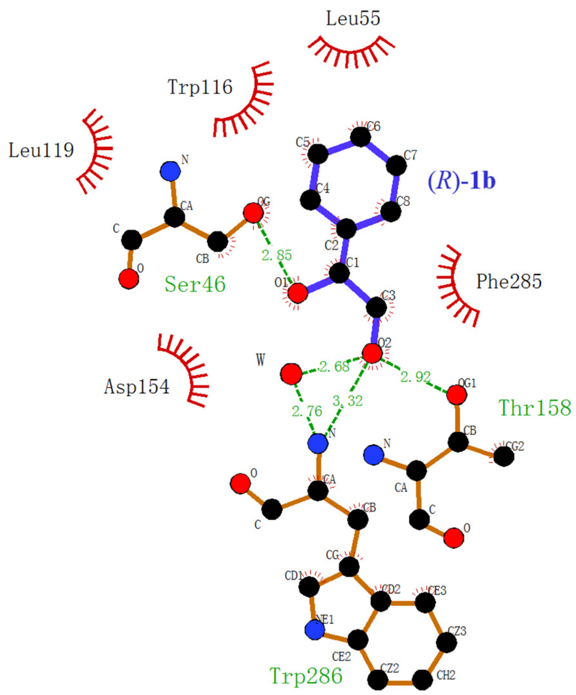

Figure S4. Interactions between (*R*)-**1b** and the amino acid residues of RCR.

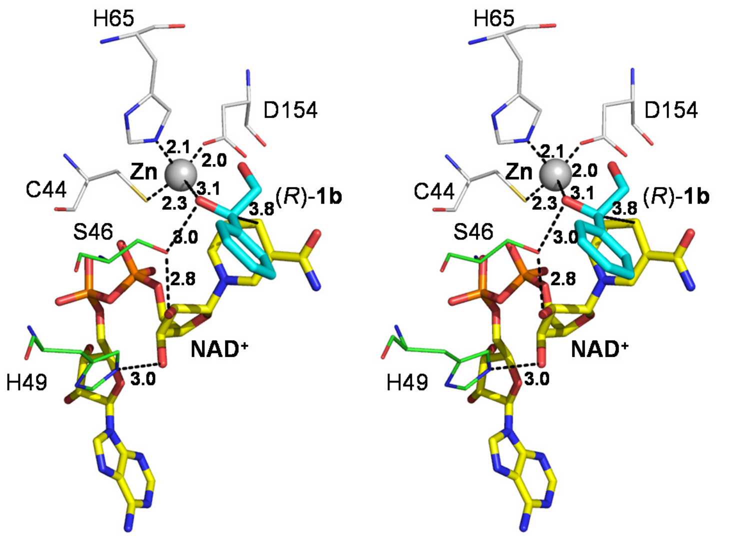

Figure S5. Catalytic mechanism of RCR based on docking model of the ternary complex with NAD^+ (yellow) and (*R*)-**1b** (cyan). The zinc ion was coordinated by Cys44, His65, Asp154 and the hydroxyl oxygen atom of (*R*)-**1b**. The proton abstracted from the alcohol substrate during catalysis was transferred to the free solvent via a proton-relay system including Ser46, the 2' OH of the nicotinamide-ribose of NAD^+, and the imidazole of His49. The *pro*-R hydrogen was directly transferred from chiral carbon of (*R*)-**1b** to C4N of the nicotinamide ring (3.8 Å distance).

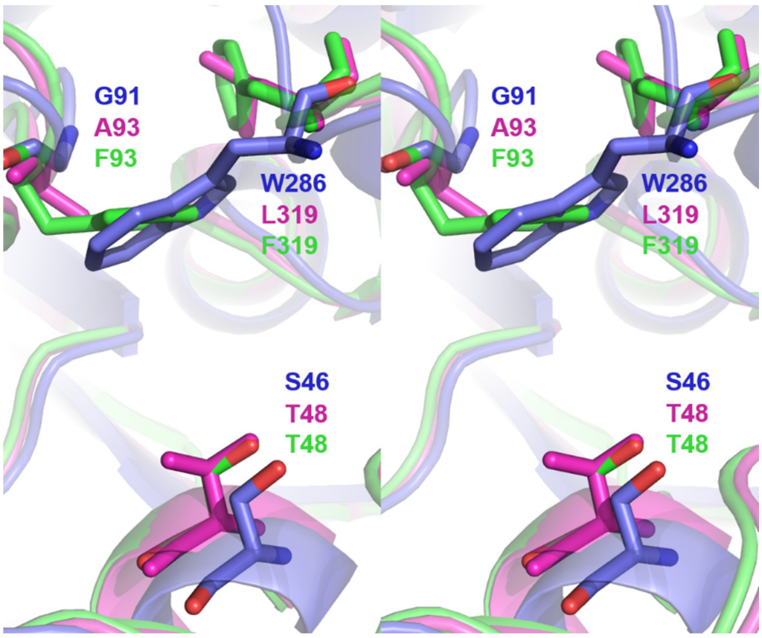

Figure S6. Structural comparison of RCR (blue) with human ADH αα (magentas) and HLADH (green) at the positions of S46, G91 and W286 in RCR.

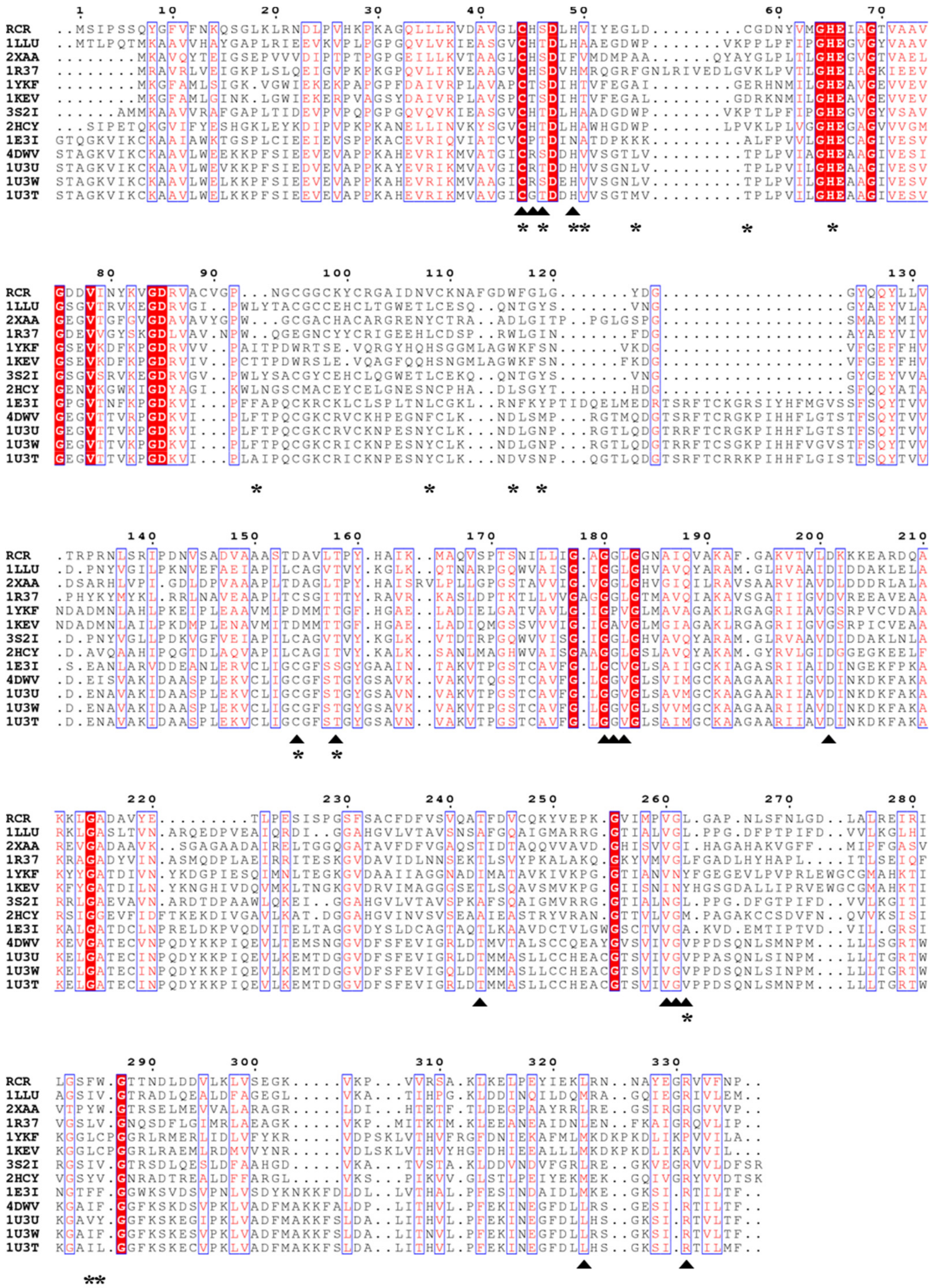

Figure S7. Multiple sequence alignment of RCR from *C. parapsilosis* and structure-solved MDRs, prepared with the program Espript (http://espript.ibcp.fr/ESPript/cgi-bin/ESPript.cgi/). 1LLU from *P. aeruginosa*, 2XAA from *R. rubber*, 1R37 from *S. solfataricus*, 1YKF from *T. brockii*, 1KEV from *C.beijerinckii*, 3S2I from *R. eutropha JMP134*, 2HCY from *S. cerevisiae*, 1E3I from *Mus musculus*, 4DWV from *Equus caballus*, 1U3U, 1U3W and 1U3T from *Homo sapiens*. Gaps in the aligned sequences were indicated by dashes. Identical amino acid residues were highlighted in red. Conserved residues were boxed with blue lines. NAD(H)-binding motifs were labeled by triangle below the amino acids, and pocket-forming amino acids were labeled by asterisk.

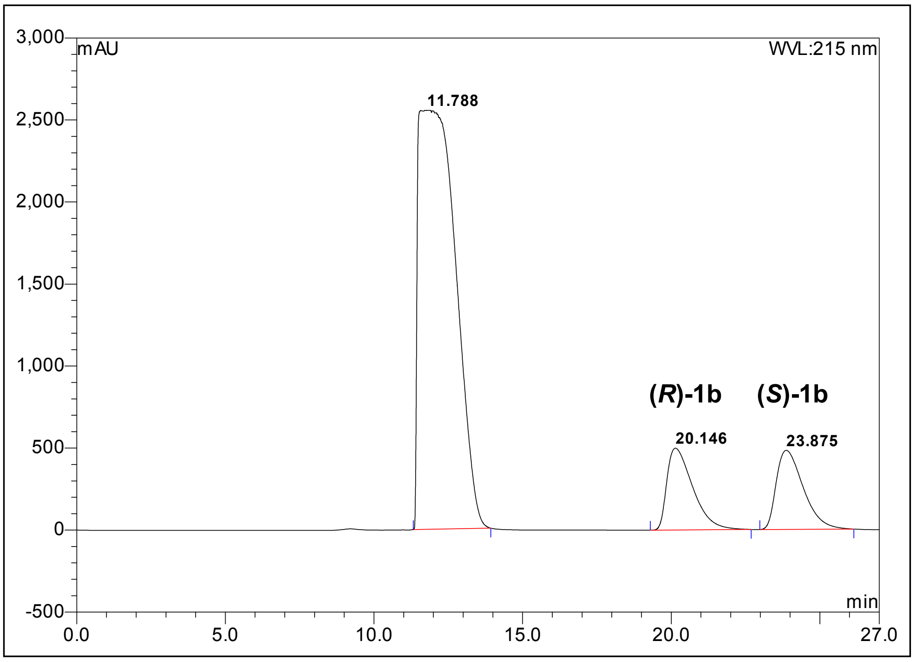

Figure S8. Determination of enantiomeric excess of **1b** by HPLC analysis: column OB-H; flow rate 0.4 ml/min; Mobile phase hexane/isopropanol (v/v) = 9:1; (R)-**1b** = 20.1 min**;** (S)-**1b** = 23.9 min.

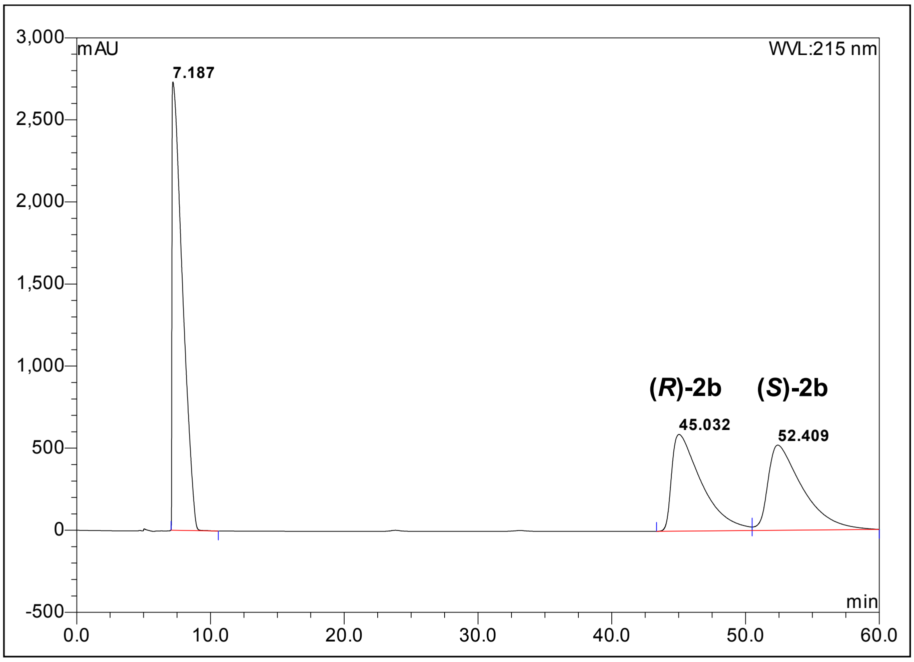

Figure S9. Determination of enantiomeric excess of **2b** by HPLC analysis: column OB-H; flow rate 0.8 ml/min; Mobile phase hexane/isopropanol (v/v) = 98:2; (R)-**2b** = 45.0 min**;** (S)-**2b** = 52.4 min.

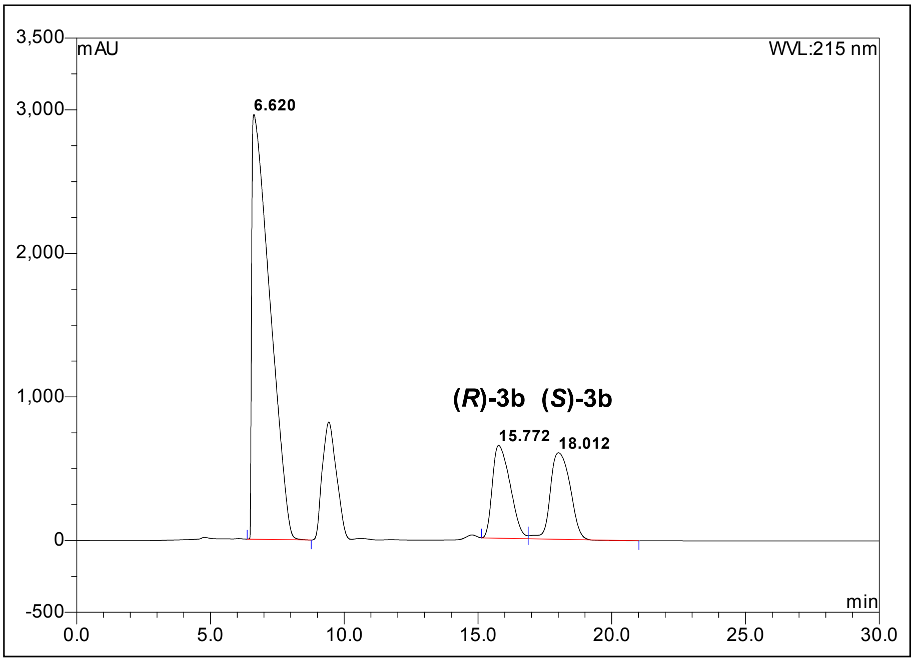

Figure S10. Determination of enantiomeric excess of **3b** by HPLC analysis: column OB-H; flow rate 0.8 ml/min; Mobile phase hexane/isopropanol (*v/v*) = 95:5; (*R*)-**3b** = 15.8 min**;** (*S*)-**3b** = 18.0 min.

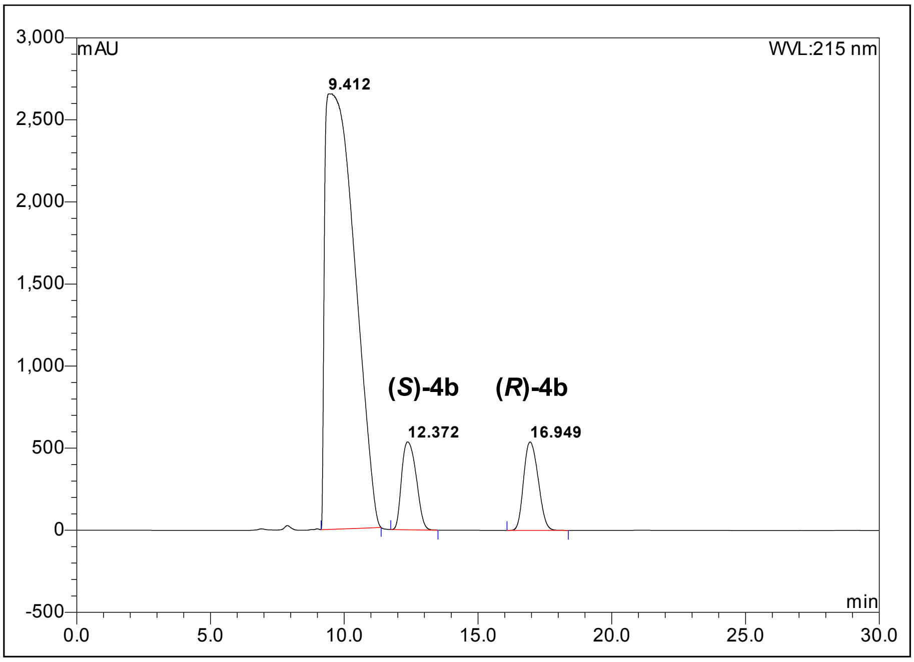

Figure S11. Determination of enantiomeric excess of **4b** by HPLC analysis: column OB-H; flow rate 0.6 ml/min; Mobile phase hexane/isopropanol (*v/v*) = 9:1; (*R*)-**4b** = 16.9 min**;** (*S*)-**4b** = 12.4 min.

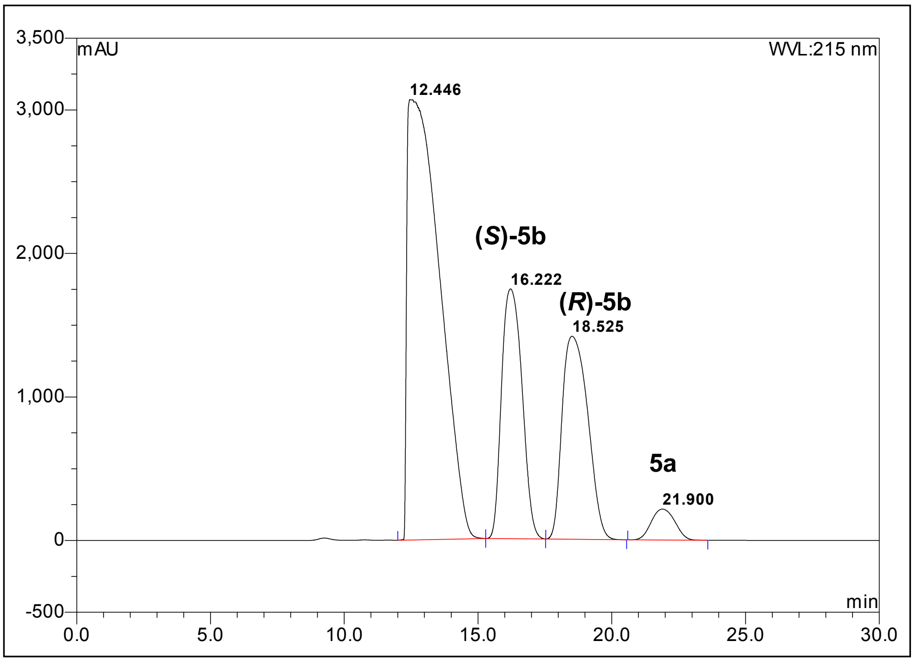

Figure S12. Determination of enantiomeric excess of **5b** by HPLC analysis: column OB-H; flow rate 0.4 ml/min; Mobile phase hexane/isopropanol (*v/v*) = 9:1; (*R*)-**5b** = 18.5 min**;** (*S*)-**5b** = 16.2 min.

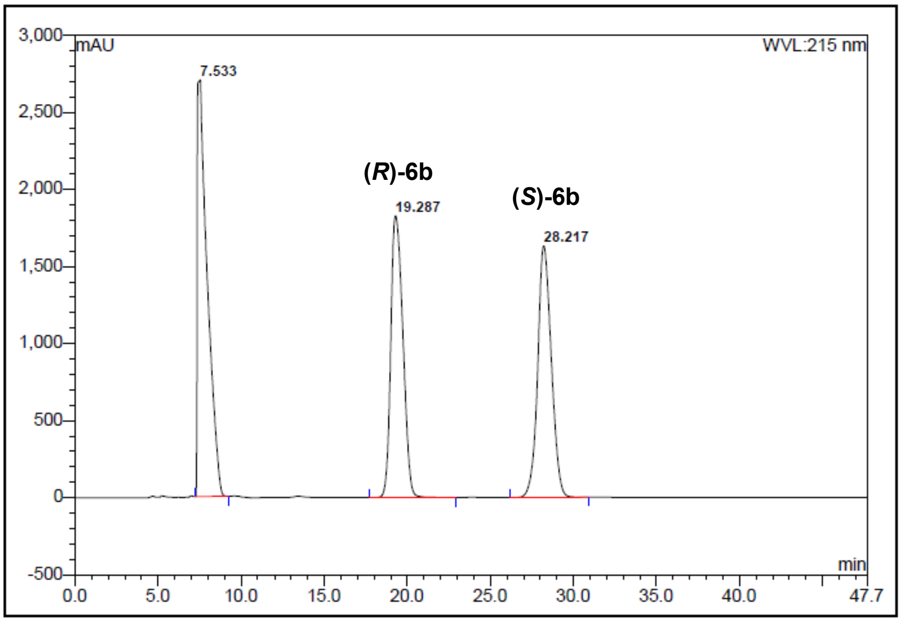

Figure S13. Determination of enantiomeric excess of **6b** by HPLC analysis: column OB-H; flow rate 0.8 ml/min; Mobile phase hexane/isopropanol (*v/v*) = 98:2; (*R*)-**6b** = 19.3 min**;** (*S*)-**6b** = 28.2 min.

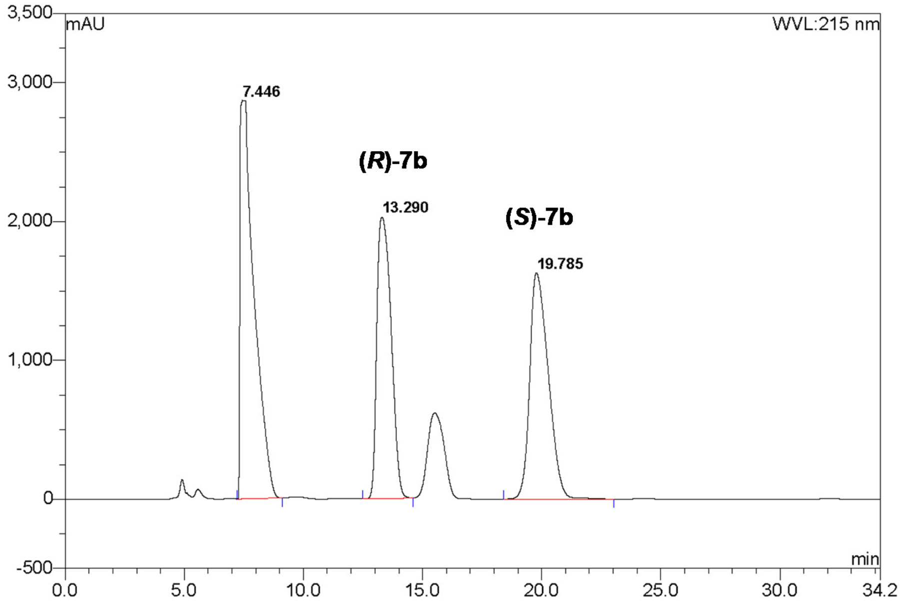

Figure S14. Determination of enantiomeric excess of **7b** by HPLC analysis: column OB-H; flow rate 0.8 ml/min; Mobile phase hexane/isopropanol (*v/v*) = 98:2; (*R*)-**7b =** 13.3 min**;** (*S*)-**7b =** 19.8 min.

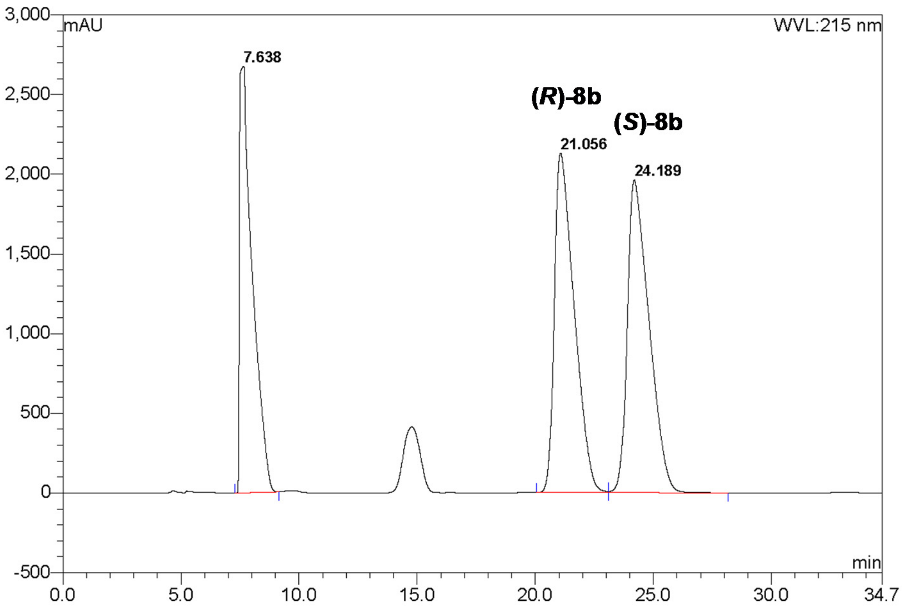

Figure S15. Determination of enantiomeric excess of **8b** by HPLC analysis: column OB-H; flow rate 0.8 ml/min; Mobile phase hexane/isopropanol (*v/v*) = 98:2; (*R*)-**8b =** 21.1 min**;** (*S*)-**8b =** 24.2 min.

11. References

1 Y. Nie, Y. Xu, H. Y. Wang, N. Xu, R. Xiao and Z. H. Sun, *Biocatal. Biotransform.*, 2008, **26**, 210-219.

2 Z. Otwinowski and W. Minor, *Methods Enzymol.*, 1997, **276**, 307-326.

3 A. T. Brunger, *Nat. Protocols*, 2007, **2**, 2728-2733; P. Emsley, B. Lohkamp, W. G. Scott and K. Cowtan, *Acta Crysta. D.*, 2010, **66**, 486-501.

4 P. Emsley and K. Cowtan, *Acta Cryst. D.*, 2004, **60**, 2126-2132.

5 P. J. Baker, K. L. Britton, M. Fisher, J. Esclapez, C. Pire, M. J. Bonete, J. Ferrer and D. W. Rice, *Proc. Natl. Acad. Sci.*, 2009, **106**, 779-784.

6 B. V. Plapp, *Arch. Biochem. Biophys.*, 2010, **493**, 3-12.

7 Y. Nie, R. Xiao, Y. Xu and G. T. Montelione, *Org. Biomol. Chem.*, 2011, **9**, 4070-4078.

8 O. Trott and A. J. Olson, *J. Comput. Chem.*, 2010, **31**, 455-461.

9 B. J. Gibbons and T. D. Hurley, *Biochemistry*, 2004, **43**, 12555-12562.

10 B. V. Plapp and S. Ramaswamy, *Biochemistry*, 2012, **51**, 4035-4048.

11 S. Svensson, J.-O. Höög, G. Schneider and T. Sandalova, *J. Mol. Biol.*, 2000, **302**, 441-453.

12 S. Pal, D.-H. Park and B. V. Plapp, *Chem. Biol. Interact.*, 2009, **178**, 16-23.

13 L. Esposito, I. Bruno, F. Sica, C. A. Raia, A. Giordano, M. Rossi, L. Mazzarella and A. Zagari, *Biochemistry*, 2003, **42**, 14397-14407; A. Pennacchio, L. Esposito, A. Zagari, M. Rossi and C. A. Raia, *Extremophiles*, 2009, **13**, 751-761.

14 M. Karabec, A. Łyskowski, K. C. Tauber, G. Steinkellner, W. Kroutil, G. Grogan and K. Gruber, *Chem. Commun.*, 2010, **46**, 6314-6316.

15 I. Levin, G. Meiri, M. Peretz, Y. Burstein and F. Frolow, *Protein Sci.*, 2004, **13**, 1547-1556.

16 E. Goihberg, M. Peretz, S. Tel-Or, O. Dym, L. Shimon, F. Frolow and Y. Burstein, *Biochemistry*, 2010, **49**, 1943-1953.

17 C. Kang, R. Hayes, E. J. Sanchez, B. N. Webb, Q. Li, T. Hooper, M. S. Nissen and L. Xun, *Mol. Microbiol.*, 2012, **83**, 85-95.

18 C. Heiss, M. Laivenieks, J. G. Zeikus and R. S. Phillips, *J. Am. Chem. Soc.*, 2001, **123**, 345-346.

19 V. B. Chen, W. B. Arendall, J. J. Headd, D. A. Keedy, R. M. Immormino, G. J. Kapral, L. W. Murray, J. S. Richardson and D. C. Richardson, *Acta Crysta. D.*, 2009, **66**, 12-21.

20 J.-C. Gelly, A. P. Joseph, N. Srinivasan and A. G. De Brevern, *Nucleic Acids Res.*, 2011, **39**, W18-W23.